environmental sciences proceedings

MDPI

Proceeding Paper

Dust Optical and Microphysical Properties of Saharan and Saudi Arabian Deserts Distributed in Europe Based on AERONET Data Products †

Elina Giannakaki [1,2,*], Eirini Verykiou [1], Eftychia Vasileiou [1] and Mika Komppula [2]

1 Department of Environmental Physics and Meteorology, University of Athens, 15784 Athens, Greece; eiriniber26@gmail.com (E.V.); eftihiavas1234@gmail.com (E.V.)
2 Atmospheric Research Centre of Eastern Finland, Finnish Meteorological Institute, 70211 Kuopio, Finland; mika.komppula@fmi.fi
* Correspondence: elina@phys.uoa.gr

† Presented at the 16th International Conference on Meteorology, Climatology and Atmospheric Physics—COMECAP 2023, Athens, Greece, 25–29 September 2023.

Abstract: This study investigates the spatial distribution of optical and microphysical dust properties in Europe and possible differences between the Saharan and Saudi Arabian deserts' dust particles based on the AERONET network. Data were collected within the period from 2001 to 2018 from 16 different stations. Pure dust conditions were identified. The Saudi Arabian lidar ratio (at 440 nm) was determined to be 53 ± 7 sr, much lower than the Saharan lidar ratio at the same wavelength, which was found to be 66 ± 10 sr. Particle depolarization ratio values at 440 nm were similar for both regions. Although our findings are consistent with earlier studies based on AERONET products, they do not agree with lidar observations. We found significantly larger lidar ratios at 440 nm both for Arabian dust (difference of 15 sr) and Saharan dust (difference of 13 sr) compared to lidar observations. These differences are smaller at 532 nm. Differences at both 440 and 532 nm between AERONET and lidar observations were on the order of 5 sr for Arabian dust and even smaller (order of 2 sr) for Saharan dust.

Keywords: desert dust particles; lidar ratio; depolarization ratio; Saharan dust; Saudi Arabian dust

Citation: Giannakaki, E.; Verykiou, E.; Vasileiou, E.; Komppula, M. Dust Optical and Microphysical Properties of Saharan and Saudi Arabian Deserts Distributed in Europe Based on AERONET Data Products. *Environ. Sci. Proc.* **2023**, *26*, 190. https://doi.org/10.3390/environsciproc2023026190

Academic Editors: Konstantinos Moustris and Panagiotis Nastos

Published: 12 September 2023

1. Introduction

Atmospheric particles have an impact on global climate variability both directly and indirectly by scattering and absorbing radiation as well as by influencing cloud formation and weather uncertainties [1,2].

According to estimates, mineral dust constitutes about one-third of the globe's aerosol loading, thus aerosol optical depth (AOD), and represents one of the most prominent aerosol types [3]. Mineral dust has an impact on the dynamics and chemistry of the atmosphere, along with air quality, public health, and visibility [4,5]. Mineral dust has a wide range of size, optical, and microphysical properties, which directly affect the impacts listed above. Therefore, rather than using a global average, those features need to be understood and evaluated on a regional scale. The primary source of mineral dust in the atmosphere is Northern Africa. This region is being examined in our research since earlier published data indicated a kind of distinction between dust from different deserts [6].

Different aerosol types can be classified using aerosol properties derived from remote sensing measurements. Using active aerosol remote sensing, the classification of mineral dust particles in the atmosphere could be accomplished using the extinction-to-backscatter (lidar) ratio (S_λ^p) and particle linear depolarization ratio (δ_λ^p) as measured by polarization-sensitive Raman or high spectral resolution lidar [7–10]. The lidar ratio provides information on the size and absorption of aerosol particles, while the particle linear depolarization ratio is an indicator of particle shape. Higher linear depolarization values indicate more spherical particles.

Furthermore, particle types can be classified using properties derived from passive aerosol remote sensing measurements. Those are used to distinguish aerosols based on their aerosol optical depth (AOD) and their spectral dependence, which can be described by the Ångström exponent [11,12]. These factors, along with the fine mode fraction (FMF) of the aerosol size distribution and single-scattering albedo (SSA) [13], allow the quantification of aerosol size and aerosol loading as well as the estimation of light-absorbing properties.

Aerosol robotic network [14] is a network of ground-based sun photometers (CIMEL spectral radiometers) that measure sun and sky radiance at a number of preset wavelengths in the visible and near-infrared spectra in order to determine the properties of atmospheric aerosols. It consists of hundreds of sites all over the globe, providing long-term aerosol datasets with quality assurance and uniform calibration. Single scattering albedo (SSA), fine-mode fraction (FMF), complex refractive index, spectral aerosol optical depth (AOD), and particle size distribution are some of the properties that are included in those datasets. Version 3 of the AERONET retrieval provides us with the lidar ratio and particle linear depolarization ratio as standard inversion products.

In this study, we compare the pure mineral dust from the Sahara Desert and Saudi Arabia's (Arabian Peninsula) desert using all the aforementioned properties derived from the AERONET version 3 inversion product.

The AERONET stations used in this research are presented in Section 2, along with a description of our methodology. In Section 3, we present and discuss our results. In Section 4, a summary and conclusions of this study are given.

2. Materials and Methods

2.1. Theoretical Background of Parameters Used

The extinction-to-backscatter (lidar) ratio can be measured directly from the particle backscatter coefficient β_λ^p and the particle extinction coefficient a_λ^p, using polarization-sensitive Raman and high spectral-resolution lidars.

$$S_\lambda^p = \frac{a_\lambda^p}{\beta_\lambda^p} \tag{1}$$

Regarding the particle linear depolarization ratio, cautious calibration of the lidar receiver measurement is required, as is measurement of the return signal in the plane of polarization perpendicular to that of transmitted polarized laser light [15,16].

$$\delta_\lambda^p = \frac{\beta_\lambda^{p,\perp}}{\beta_\lambda^{p,\parallel}} \tag{2}$$

This parameter is sensitive to particle shape [17]. Nonspherical particles are represented by values of δ between 0.30 and 0.35 (pure mineral dust, volcanic ash), while values near zero denote the presence of spherical particles. Direct solar radiation and sky radiation are both measured by AERONET sun/sky radiometers. Automatic analysis of the collected data is performed using the AERONET inversion algorithm [18]. The retrieved aerosol products are available from the AERONET database [19] https://aeronet.gsfc.nasa.gov/ (accessed on 19 December 2022). The spectral particle linear depolarization ratios and lidar ratios were added to the list of standard inversion products, which also includes the single-scattering albedo, the particle size distribution, and the complex refractive index of the observed particles.

For each observation, the Müller scattering matrix's [20] elements F_{11}, λ (r, n) and F_{22}, λ (r, n) are calculated using the inferred particle size distribution and refractive index n = nr + i·ni from the AERONET inversion product. When incident light is unpolarized, the element F_{11}, λ (r, n) is proportionate to the flux of scattered light, whereas F_{22}, λ (r, n) is highly dependent on the angular and spectral distribution of the radiative intensity [20]. From the element F_{11}, λ (r, n) at the scattering angle of 180° and the simultaneously inferred single-scattering albedo (ω_λ), the lidar ratio can be computed as:

$$S_\lambda^p = \frac{4\pi}{\omega_\lambda F_{11}, \lambda(r, n, 180^\circ)} \quad (3)$$

The particle linear depolarization ratio is calculated by the elements F_{11}, λ (r, n) and F_{22}, λ (r, n) at a scattering angle of 180° as:

$$\delta_\lambda^p = \frac{1 - \frac{F_{22,\lambda}(r, n, 180^\circ)}{F_{11,\lambda}(r, n, 180^\circ)}}{1 + \frac{F_{22,\lambda}(r, n, 180^\circ)}{F_{11,\lambda}(r, n, 180^\circ)}} \quad (4)$$

2.2. Location and Data Selection

To explore the differences between Saharan and Saudi Arabian desert particles, we selected 16 AERONET sites. Six of them are representative of the Arabian desert: SEDE BOKER (30.855° N, 34.782° E), Eilat (29.503° N, 34.917° E), KAUST_Campus (22.305° N, 39.103° E), Solar_Village (24.907° N, 46.397° E), Mezaira (23.105° N, 53.755° E), and Masdar_Institute (24.442° N, 54.617° E). As for the Saharan desert, the following stations were selected to serve as an effective representation of the extent of this desert: Saada (31.626° N, 8.156° W), Oujda (34.653° N, 1.898° W), Blida (36.508° N, 2.881° E), IER_Cinzana (13.278° N, 5.934° W), Agoufou (15.345° N, 1.479° W), Banizoumbou (13.547° N, 2.665° E), Zinder_Airport (13.777° N, 8.990° E), Tamanrasset_INM (22.790° N, 5.530° E), El_Farafra (27.058° N, 27.990° E), and Cairo_EMA_2 (30.081° N, 31.290° E). In order to achieve the most accurate results, the sites were selected depending on their location and time availability. We consider all version 3 level 2.0 observations that were available in December 2022. AERONET inversions are only performed for observations with an AOD larger than 0.4 at 440 (Dubovik et al., 2006). To ensure that the resulting values are an accurate representation of pure dust conditions (i.e., undiluted dust plumes), the AERONET inversion products that are accessible for the stations mentioned above have been filtered. In this study, we set as thresholds an AOD greater than or equal to 0.4 at 440 nm [18] and a 440/870 nm Ångström exponent ($Å_{440/870}$) value less than 0.2 [21] to retain high accuracy and minimize interference of non-dust aerosols, despite the fact that fine mode dust might also be eliminated. The Saharan desert has a higher percentage of pure dust cases out of all observations than the Arabian desert has.

3. Results

The results of our research based on AERONET version 3 products for pure mineral dust are displayed in Table 1. The linear depolarization ratio, the lidar ratio, the complex refractive index, and the single-scattering albedo are listed in this table along with their medians, means, and standard deviations at four wavelengths for each region under study. Additionally, it provides information on the number of pure dust cases that are currently available, the mean and median values of $Å_{(440/870)}$, fine mode fraction, and coarse-mode effective radius found for the Arabian and Saharan deserts.

Table 1. Mean values, standard deviation, and range of values of the AERONET-derived δ, S, refractive index (n= n_r + in_i) and the single scattering albedo (ω) at 440, 675, 870, and 1020 nm, together with the number of pure dust cases (N), as well as the Ångström exponent (440–870 nm), fine-mode fraction (FMF), and coarse-mode effective radius (r_c) for Saharan and Saudi Arabian desert dust particles.

	Arabian Mean ± STD	**Arabian Range**	**Saharan Mean ± STD**	**Saharan Range**
N	2251		6026	
$Å_{440/870}$	0.11 ± 0.06	0.06–0.2	0.11 ± 0.06	0.06–0.2
FMF	0.07 ± 0.02	0.02–0.19	0.07 ± 0.02	0.01–0.2
r_c (μm)	1.78 ± 0.15	1.35–2.91	1.80 ± 0.18	1.34–3.65
$δ_{440}$ (%)	22.3 ± 2.5	5–30	23.8 ± 3.0	1–30
$δ_{675}$ (%)	26.5 ± 1.9	6–30	28.2 ± 2.2	1–30
$δ_{870}$ (%)	28.7 ± 2.2	7–30	30.5 ± 2.4	1–40
$δ_{1020}$ (%)	30.0 ± 2.5	5–30	31.8 ± 2.7	1–40
S_{440} (sr)	53 ± 7	19–148	66 ± 10	14–169
S_{675} (sr)	39 ± 4	15–63	47 ± 7	16–81
S_{870} (sr)	41 ± 5	18–65	50 ± 7	19–86
S_{1020} (sr)	44 ± 6	19–72	53 ± 8	20–93
$n_{r,\,440}$	1.52 ± 0.04	1.40–1.60	1.48 ± 0.05	1.34–1.60
$n_{r,\,675}$	1.52 ± 0.03	1.43–1.60	1.48 ± 0.04	1.37–1.60
$n_{r,\,870}$	1.50 ± 0.03	1.41–1.60	1.46 ± 0.04	1.35–1.60
$n_{r,\,1020}$	1.49 ± 0.04	1.39–1.60	1.45 ± 0.04	1.33–1.60
$n_{i,\,440}$	0.0033 ± 0.0008	0.001–0.015	0.0038 ± 0.0013	0.0007–0.033
$n_{i,\,675}$	0.0008 ± 0.0004	0.0005–0.004	0.0010 ± 0.0008	0.0005–0.011
$n_{i,\,870}$	0.0008 ± 0.0005	0.0005–0.007	0.0010 ± 0.0009	0.0005–0.014
$n_{i,\,1020}$	0.0009 ± 0.0007	0.0005–0.006	0.0011 ± 0.0012	0.0005–0.017
$ω_{440}$	0.91 ± 0.02	0.75–0.96	0.90 ± 0.02	0.69–0.98
$ω_{675}$	0.98 ± 0.01	0.91–0.99	0.98 ± 0.02	0.84–0.99
$ω_{870}$	0.98 ± 0.01	0.92–0.99	0.98 ± 0.02	0.84–0.99
$ω_{1020}$	0.98 ± 0.01	0.92–0.99	0.98 ± 0.02	0.82–0.99

While the Ångstrom exponent and FMF values are comparable between the two areas, the coarse-mode effective radius varies slightly between them, with the Saharan desert region having a slightly higher value than the Arabian region. These outcomes are a result of our selection of coarse-mode aerosol data.

The mean and median values of the lidar ratio demonstrate an interesting contrast, with Saharan values being significantly greater than Arabian values. More specifically, spectral lidar ratio mean values range from 41 to 53 sr for the Arabian desert and from 47 to 66 sr for the Saharan desert. Those differences are attributed to the different chemical composition of the dust particles in the aforementioned areas [22].

In accordance with spectral linear depolarization values, the Saharan desert has mean values that are slightly higher than the Arabian Peninsula's. These mean values range from 22.3% to 30.0% and 23.8% to 31.8%, respectively, for the two deserts. The values of spectral δ vary between 5 and 30% for Arabian dust and between 1 and 40% for Saharan dust. The maximum of the δ distribution decreases as the wavelength decreases and is highest for the Saharan dust.

There are also discrepancies in the real-part mean and median values of the complex refractive index, n_r, with the Saharan desert possessing lower values than the Arabian Peninsula. Their respective mean spectral values vary between 1.45 and 1.48, as well as between 1.49 and 1.52, but do not show clear wavelength dependence.

The imaginary part, ni, mean and median values of the refractive index vary as well, with the Saharan desert's values being higher than the Arabian desert's, indicating that Saharan dust is more absorbing than Arabian dust. Their mean spectral values vary between 0.0010 and 0.0038, along with 0.0008 and 0.0033, respectively.

4. Conclusions

In this study, we investigated the particle linear depolarization ratio δ and the particle lidar ratio S as provided in the recently released version 3 of the AERONET inversion. To select observations of pure mineral dust conditions, only AERONET with a 440/870 Ångström exponent ($Å_{440/870}$) value less than 0.2 and AOD greater than or equal to 0.4 at 440 nm were selected. The AERONET stations considered here were chosen according to their location and are assumed to represent observations of mineral dust from the Saharan and Arabian Peninsulas.

The mean depolarization ratio value, δ, is slightly larger for the Saharan dust compared to the Arabian dust for all wavelengths. The larger the wavelength, the larger the difference. Spectral lidar ratio mean values range from 41 to 53 sr for the Arabian desert and from 50 to 66 sr for the Saharan desert. The differences are attributed to the different chemical compositions of the dust particles in the two deserts.

In Figure 1, we present the results of lidar ratio (a) and depolarization ratio (b) for this study (asterisk) compared to an earlier lidar study [23] (square) and sunphotometer AERONET study [6] (triangle) both in the Saharan (red) and Arabian (blue) regions. Our findings are consistent with earlier studies based on AERONET products [6]. Specifically, differences in lidar ratio values of only 1 to 3 sr are found between this study and in [6]. Also, we observe the same spectral dependence. For the depolarization ratio, we found slightly larger values of the order of 2% for Arabian dust, while for Saharan dust, the values are almost the same.

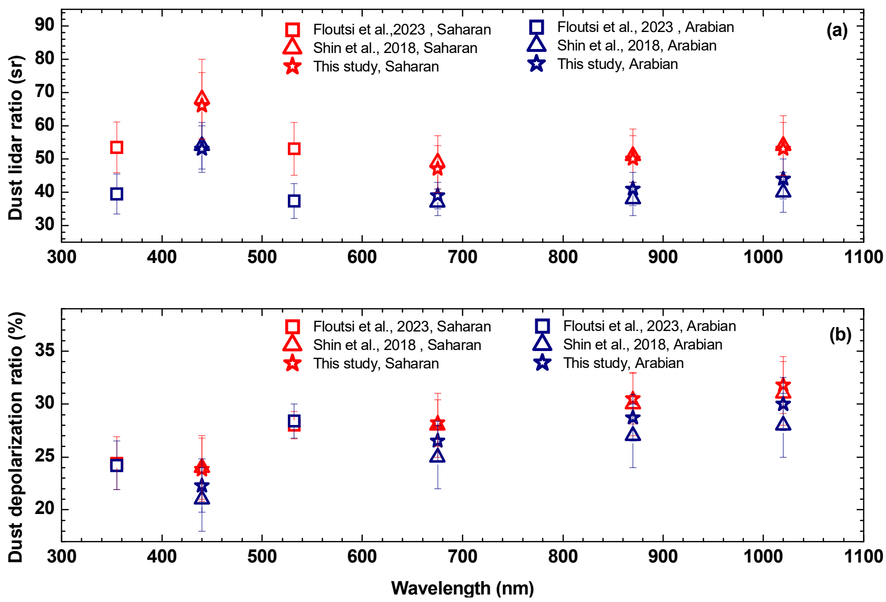

Figure 1. Spectral wavelength dependence of lidar ratio and depolarization ratio based on this study (asterisk) for Saharan (red) and Arabian dust (blue). For comparison, lidar [23] (square) and sunphotometer [6] (triangle)-based results have also been included.

However, sunphotometer products of lidar ratio and depolarization ratio do not agree with lidar observations [23]. We found significantly larger lidar ratios at 440 nm both for Arabian dust (difference of 15 sr) and Saharan dust (difference of 13 sr) compared to lidar observations. These differences are smaller at 532 nm. Differences at both 440 and 532 nm between AERONET and lidar observations were on the order of 5% for Arabian dust and even smaller (order of 2%) for Saharan dust. We cannot currently understand and explain the reason for the discrepancy between sunphotometer AERONET products and lidar products, especially for lidar ratio values.

Author Contributions: E.G. developed the methodology and wrote the article. E.V. (Eirini Verykiou) and E.V. (Eftychia Vasileiou) performed the AERONET data analysis. M.K. participated in scientific discussions on this study. All authors reviewed and edited the article during its preparation process. All authors have read and agreed to the published version of the manuscript.

Funding: The research work was supported by the Hellenic Foundation for Research and Innovation (H.F.R.I.) Research Projects to support Faculty members and Researchers and the procurement of high-cost research equipment grant (Project Number: 2544).

Institutional Review Board Statement: Not applicable.

Informed Consent Statement: Not applicable.

Data Availability Statement: The data are available upon request from the authors.

Conflicts of Interest: The authors declare no conflict of interest.

References

1. Stevens, B.; Feingold, G. Untangling aerosol effects on clouds and precipitation in a buffered system. *Nature* **2009**, *461*, 607–613. [CrossRef] [PubMed]
2. Boucher, O.; Randall, D.; Artaxo, P.; Bretherton, C.; Feingold, G.; Forster, P.; Kerminen, V.M.; Kondo, Y.; Liao, H.; Lohmann, U.; et al. Clouds and Aerosols. In *Climate Change 2013—The Physical Science Basis*; Cambridge University Press: Cambridge, UK, 2013; pp. 571–658.
3. Kinne, S.; Schulz, M.; Textor, C.; Guibert, S.; Balkanski, Y.; Bauer, S.E.; Berntsen, T.; Berglen, T.F.; Boucher, O.; Chin, M.; et al. An AeroCom initial assessment—Optical properties in aerosol component modules of global models. *Atmos. Chem. Phys.* **2006**, *6*, 1815–1834. [CrossRef]
4. Jickells, T.; An, Z.; Andersen, K.K.; Baker, A.; Bergametti, G.; Brooks, N.; Cao, J.; Boyd, P.; Duce, R.; Hunter, K. Global iron connections between desert dust, ocean biogeochemistry, and climate. *Science* **2005**, *308*, 67–71. [CrossRef] [PubMed]
5. Davidson, C.I.; Phalen, R.F.; Solomon, P.A. Airborne Particulate Matter and Human Health: A Review. *Aerosol Sci. Technol.* **2005**, *39*, 737–749. [CrossRef]
6. Shin, S.; Tesche, M.; Kim, K.; Kezoudi, M.; Tatarov, B.; Müller, D.; Noh, Y. On the spectral depolarisation and lidar ratio of mineral dust provided in the AERONET version 3 inversion product. *Atmos. Chem. Phys.* **2018**, *18*, 12735–12746. [CrossRef]
7. Müller, D.; Ansmann, A.; Mattis, I.; Tesche, M.; Wandinger, U.; Althausen, D.; Pisani, G. Aerosol-type-dependent lidar ratios observed with Raman lidar. *J. Geophys. Res.* **2007**, *112*, D16202. [CrossRef]
8. Burton, S.P.; Ferrare, R.A.; Hostetler, C.A.; Hair, J.W.; Rogers, R.R.; Obland, M.D.; Butler, C.F.; Cook, A.L.; Harper, D.B.; Froyd, K.D. Aerosol classification using airborne High Spectral Resolution Lidar measurements—Methodology and examples. *Atmos. Meas. Tech.* **2012**, *5*, 73–98. [CrossRef]
9. Burton, S.P.; Ferrare, R.A.; Vaughan, M.A.; Omar, A.H.; Rogers, R.R.; Hostetler, C.A.; Hair, J.W. Aerosol classification from airborne HSRL and comparisons with the CALIPSO vertical feature mask. *Atmos. Meas. Tech.* **2013**, *6*, 1397–1412. [CrossRef]
10. Groß, S.; Esselborn, M.; Weinzierl, B.; Wirth, M.; Fix, A.; Petzold, A. Aerosol classification by airborne high spectral resolution lidar observations. *Atmos. Chem. Phys.* **2013**, *13*, 2487–2505. [CrossRef]
11. Giles, D.M.; Holben, B.N.; Eck, T.F.; Sinyuk, A.; Smirnov, A.; Slutsker, I.; Dickerson, R.; Thompson, A.; Schafer, J. An analysis of AERONET aerosol absorption properties and classifications representative of aerosol source regions. *J. Geophys. Res.* **2012**, *117*, D17203. [CrossRef]
12. Schuster, G.L.; Dubovik, O.; Holben, B.N. Angstrom exponent and bimodal aerosol size distributions. *J. Geophys. Res.* **2006**, *111*, D07207. [CrossRef]
13. Lee, J.; Kim, J.; Song, C.; Kim, S.; Chun, Y.; Sohn, B.; Holben, B. Characteristics of aerosol types from AERONET sunphotometer measurements. *Atmos. Environ.* **2010**, *44*, 3110–3117. [CrossRef]
14. Holben, B.N.; Eck, T.F.; Slutsker, I.; Tanré, D.; Buis, J.; Setzer, A.; Vermote, E.; Reagan, J.; Kaufman, Y.J.; Nakajima, T. AERONET—A federated instrument network and data archive for aerosol characterization. *Remote Sens. Environ.* **1998**, *66*, 1–16. [CrossRef]
15. Freudenthaler, V.; Esselborn, M.; Wiegner, M.; Heese, B.; Tesche, M.; Ansmann, A.; Müller, D.; Althausen, D.; Wirth, M.; Fix, A. Depolarization ratio profiling at several wavelengths in pure Saharan dust during SAMUM 2006. *Tellus B* **2009**, *61*, 165–179. [CrossRef]
16. Freudenthaler, V. About the effects of polarising optics on lidar signals and the Δ90 calibration. *Atmos. Meas. Tech.* **2016**, *9*, 4181–4255. [CrossRef]
17. Shin, S.-K.; Tesche, M.; Müller, D.; Noh, Y. Technical note: Absorption aerosol optical depth components from AERONET observations of mixed dust plumes. *Atmos. Meas. Tech.* **2019**, *12*, 607–618. [CrossRef]

18. Dubovik, O.; Sinyuk, A.; Lapyonok, T.; Holben, B.N.; Mishchenko, M.; Yang, P.; Eck, T.F.; Volten, H.; Muñoz, O.; Veihelmann, B. Application of spheroid models to account for aerosol particle nonsphericity in remote sensing of desert dust. *J. Geophys. Res.-Atmos.* **2006**, *111*, D11208. [CrossRef]
19. AERONET Database. Available online: https://aeronet.gsfc.nasa.gov/ (accessed on 19 December 2022).
20. Bohren, C.; Huffman, D. *Absorbing and Scattering of Light by Small Particles*; Wiley: Weinheim, Germany, 1983. [CrossRef]
21. Kim, D.; Chin, M.; Yu, H.; Eck, T.F.; Sinyuk, A.; Smirnov, A.; Holben, B.N. Dust optical properties over North Africa and Arabian Peninsula derived from the AERONET dataset. *Atmos. Chem. Phys.* **2011**, *11*, 20181–20201. [CrossRef]
22. Filioglou, M.; Giannakaki, E.; Backman, J.; Kesti, J.; Hirsikko, A.; Engelmann, R.; O'Connor, E.; Leskinen, J.T.; Shang, X.; Korhonen, H.; et al. Optical and geometrical aerosol particle properties over the United Arab Emirates. *Atmos. Chem. Phys.* **2020**, *20*, 8909–8922. [CrossRef]
23. Floutsi, A.A.; Baars, H.; Engelmann, R.; Althausen, D.; Ansmann, A.; Bohlmann, S.; Heese, B.; Hofer, J.; Kanitz, T.; Haarig, M.; et al. DeLiAn—A growing collection of depolarization ratio, lidar ratio and Ångström exponent for different aerosol types and mixtures from ground-based lidar observations. *Atmos. Meas. Tech.* **2023**, *16*, 2353–2379. [CrossRef]